

## Statistical Thermodynamics of Membrane Bending-Mediated Protein–Protein Attractions

Tom Chou,\* Ken S. Kim,<sup>†</sup> and George Oster<sup>‡</sup>

\*Department of Biomathematics, UCLA School of Medicine, Los Angeles, California 90095, USA, <sup>†</sup>Departments of Physiology and Applied Mathematics and Theoretical Physics, University of Cambridge, Cambridge CB3 9EW, United Kingdom, and <sup>‡</sup>Department of Molecular and Cell Biology, University of California, Berkeley, California 94720, USA

**ABSTRACT** Highly wedge-shaped integral membrane proteins, or membrane-adsorbed proteins can induce long-ranged deformations. The strain in the surrounding bilayer creates relatively long-ranged forces that contribute to interactions with nearby proteins. In contrast, to direct short-ranged interactions such as van der Waal's, hydrophobic, or electrostatic interactions, both local membrane Gaussian curvature and protein ellipticity can induce forces acting at distances of up to a few times their typical radii. These forces can be attractive or repulsive, depending on the proteins' shape, height, contact angle with the bilayer, and a pre-existing local membrane curvature. Although interaction energies are not pairwise additive, for sufficiently low protein density, thermodynamic properties depend only upon pair interactions. Here, we compute pair interaction potentials and entropic contributions to the two-dimensional osmotic pressure of a collection of noncircular proteins. For flat membranes, bending rigidities of  $\sim 100k_B T$ , moderate ellipticities, and large contact angle proteins, we find thermally averaged attractive interactions of order  $k_B T$ . These interactions may play an important role in the intermediate stages of protein aggregation. Numerous biological processes where membrane bending-mediated interactions may be relevant are cited, and possible experiments are discussed.

### INTRODUCTION

Many cellular processes require the association or dissociation of membrane proteins, especially those involved in cell signaling. Dimerization of receptors and their interactions with G-proteins, often initiated by ligand binding, require the building blocks to be in close proximity on the cell membrane (Alberts et al., 1994). Proteins associated with membrane fusion also act cooperatively (Stegmann et al., 1989). Membrane-associated proteins interact directly via screened electrostatic, van der Waal's, and hydrophobic forces. These are short ranged, operating typically over distances of a few Angstroms. In this paper, we explore how proteins can also interact indirectly via the bilayer in which they are dissolved. In particular, a protein that is "geometrically mismatched" to the bilayer will induce deformations that affect neighboring proteins. These "solvent-induced forces" (the membrane lipids being the solvent) are generated by bending deformations of the bilayer and typically act over a few nanometers.

By "geometric mismatch," we refer to any property of membrane proteins, integral, or adsorbed, that causes local bilayer bending. This effect may arise from wedge-shaped integral membrane proteins, membrane partially wrapped around adsorbed macromolecules (Koltover et al., 1999), or integral membrane proteins with large floppy cytoplasmic domains (Lipowsky et al., 1998). Provided that membrane-

associated proteins induce sufficient bilayer deformation, they can aggregate. Membrane proteins involved in electronic energy transfer, such as photoreaction centers, appear to be shaped in a way as to produce substantial membrane deformations. Additional experimental examples include aquaporin AQP1 and CD59, which aggregate to tips of pipette-drawn lipid tubules (Cho et al., 1999; Discher and Mohandas, 1996). Many membrane proteins are also non-circular in the plane of the membrane, including adsorbed polypeptides such as MARCKS (Myat et al., 1997), and bacteriorhodopsin (Luecke et al., 1999), which consists of seven transmembrane helices arranged in an elliptical configuration. Small clusters of molecules themselves, such as dimers or droplets of e.g., cholesterol or specific lipids, can, themselves, behave effectively as membrane inclusions. Droplets need not be rigid to induce membrane-mediated forces among themselves.

Previous studies of protein–protein interactions found an  $r^{-4}$  repulsion between two identical inclusions (Goulian et al., 1993; Kim et al., 1998; Park and Lubensky, 1996; Dommersnes et al., 1998). Goulian et al. (1993) and Golestanian et al. (1996) also found a weak attractive ( $-k_B T/r^4$ ) interaction arising from Casimir forces resulting from suppressed thermodynamic fluctuations of the intervening membrane. Dommersnes and Fournier (1999) have performed Monte Carlo simulations to find possible aggregation structures. They assumed that each membrane protein imposes a local curvature on the membrane. Here, we study in detail a direct mechanical origin for protein–protein attractive interactions. Although bending-induced forces between multiple inclusions are not pairwise additive, (Kim et al., 1998, 1999; Park and Lubensky, 1996; Dommersnes et al., 1998) we shall restrict ourselves to low protein densities

Received for publication 21 December 1999 and in final form 3 October 2000.

Address reprint requests to Tom Chou, Dept. of Biomathematics, AV-611/CHS, UCLA School of Medicine, Los Angeles, CA 90095. Tel.: 310-206-2787; Fax: 310-825-8685; E-mail: tomchou@ucla.edu.

© 2001 by the Biophysical Society

0006-3495/01/03/1075/13 \$2.00

where, statistically, only pairwise interactions are relevant. We find that the interplay between protein shape (Kim et al., 1999) and background Gaussian curvature dramatically affect protein–protein attractions and thermodynamics. A number of interesting features arise when we consider thermal rotational averaging of the proteins, suggesting mechanisms of protein dimerization and function.

In the next section, we briefly review the mechanical theory of inclusion-induced bilayer bending (Helfrich, 1973; Kim et al., 1998; Netz and Pincus, 1995). The lipid membrane is approximated by a thin plate that resists out-of-plane bending. Inclusions such as integral membrane proteins, or surface adsorbed molecules, impose boundary conditions along the contact line between the membrane and the protein. Using elastic plate theory to describe the membrane deformations, we derive the energy for two identical inclusions as a function of their relative position within the membrane surface.

In the following section, we show that the rotational and translational time scales can be separated so that we can thermally average out the fast rotational degrees of freedom. The resulting effective potential between two proteins is attractive, provided that the inclusions are sufficiently non-circular. We use the effective potential to compute the second virial coefficient and show how the attractive interactions affect the two-dimensional (2D) protein osmotic pressure. Finally, we discuss biological processes where membrane-induced long-ranged protein–protein attractions may play an intermediate role, and propose possible measurements.

## MEMBRANE INCLUSIONS AND HEIGHT DEFORMATION

Small membrane deformations (on the scale of the lipid or protein molecules) can be accurately modeled using standard plate theory (Landau and Lifshitz, 1985; Helfrich, 1973)

$$\tilde{E}[H(\mathbf{S}), K(\mathbf{S})] = 2b \oint d\mathbf{S} H^2(\mathbf{S}) + b_g \oint d\mathbf{S} K(\mathbf{S}), \quad (1)$$

where  $H(\mathbf{S})$  and  $K(\mathbf{S})$  are the local mean and Gaussian curvatures, and  $b$  and  $b_g$  are their associated elastic moduli. We have assumed a symmetric bilayer and a vanishing spontaneous mean curvature in the absence of the membrane-deforming proteins. For uniform  $b_g$ , the Gaussian contribution (the second integral in Eq. 1), when integrated over the entire surface, yields a constant that is independent of the relative positions of the embedded proteins (Kim et al., 1998; Struik, 1961). Thus, the Gaussian energy term can be ignored when considering protein–protein interaction energies.

Expanding the free energy about that of a flat interface,  $H(\mathbf{S}) \approx \frac{1}{2} \nabla^2 h(x, y)$ , where  $\nabla^2$  is the two-dimensional, in-plane Laplacian, and  $h(x, y)$  is a small, slowly varying height deformation from the flat state (cf., Fig. 1). Minimizing  $\tilde{E}[h(\mathbf{S})]$  with respect to  $h(x, y \in \mathbf{S})$  yields the biharmonic equation

$$\nabla^4 h(x, y) = 2\nabla^2 H(\mathbf{r}) = 0. \quad (2)$$

First, consider membrane deformations about an isolated, circularly symmetric inclusion of radius  $a$ . If the bilayer midplane contacts the protein perimeter  $\mathbf{C}$  (see Fig. 1) at a slope  $\gamma$ , the appropriate solution to Eq. 2 is  $h(r) = -\gamma \ln(r/a)$  for  $r > a$ . (The contact slope  $\gamma$  incorporates the details of the molecular interactions between the included/adsorbed protein with the lipid molecules. Molecular dynamics simulations of the local chemistry can quantitatively determine  $\gamma$ , but is beyond the scope of this paper. We will estimate  $\gamma$  from e.g., X-ray crystal structures.) In contrast to lipid compression-mediated interactions (Nielsen et al., 1998), the absence of an intrinsic length scale in Eq. 2 yields the long-ranged ( $\ln r$ ) deformation necessary for nonpairwise interactions. We have excluded terms in  $h(r)$  of the form  $r^2 \ln r$ ,  $r^2$ ,  $\text{const.}$  because they are unbounded in energy (Eq. 1), or do not satisfy the contact angle boundary condition at  $r = a$ . Because  $\nabla^2 \ln(r/a) = 2H(r) = 0$  for  $r > a$ , there is no mean curvature bending energy (proportional to  $b$ ) residing in the bilayer. In the absence of spontaneous curvature, the energy of inserting a membrane protein arises only from the hydrophobic matching between the lateral protein exterior and the aliphatic lipid tails of the bilayer (Dan and Safran, 1995). Thus, large contact angles of integral membrane proteins can be supported because bending induces no energy that would tend to eject the membrane protein. However, when interfacial tension is included (for nonflaccid membranes), the insertion of a tilted membrane

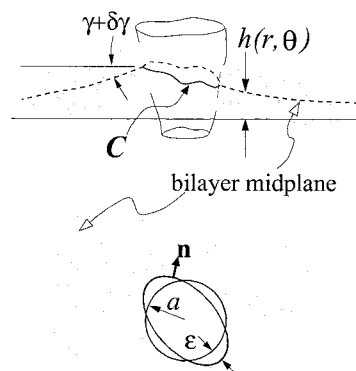


FIGURE 1 Schematic of a protein inclusion. The top figure is a cut-away view of a membrane protein that contacts the continuum bilayer midplane on curve  $\mathbf{C}$ . The contact slope on  $\mathbf{C}$  is denoted  $\gamma + \delta\gamma$ , whereas the bilayer deviation from a reference flat state is  $h(\mathbf{r})$ . The bottom picture shows a possible ellipticity  $\epsilon$  in the projection of  $\mathbf{C}$  onto the midplane.

protein forces a deformation of the membrane against its preferred flat state. Another force that may tend to eject integral proteins arises from clamped boundary conditions externally applied at some distance from the inclusion. To match such a boundary condition, the terms  $r^2 \ln r$ ,  $r^2$  are required as part of the solution for  $h(r)$ , the mean curvature no longer vanishes, and inserting an inclusion with  $\gamma \neq 0$  costs bending energy. We shall not consider these forces here. Therefore, only tension or clamped boundary conditions can destabilize and possibly eject integral proteins against their hydrophobic solvation energy in bulk water. Other effects, such as varying lipid thickness and lipid mixtures, can also contribute to the effective hydrophobic matching energy. Here, protein–membrane associations need only last long enough for bending-mediated interactions to be felt.

Next, we consider cases where more than one inclusion are present, or where the contact angles, heights of contact, or the shapes of the membrane-associated proteins are noncircular. Three types of noncircularity can arise. The inclusion itself may be noncircular (e.g., elliptical), the height of the contact curve of the bilayer midplane to the inclusion may vary along the perimeter  $\mathbf{C}$  of the protein, and the contact slope itself may vary along  $\mathbf{C}$ . These noncircular boundary effects arise from the detailed microscopic nature of the protein and its interaction with the lipid molecules. When more than one protein is present, the deformations surrounding each protein are not circularly symmetric. A nonvanishing mean curvature,  $H(\mathbf{r})$ , that gives bounded bending energies can be represented by a multipole expansion,

$$H(r, \theta) = \sum_{n=2}^{\infty} r^{-n} (a_n \cos n\theta + b_n \sin n\theta), \quad (3)$$

where  $(r, \theta)$  is the radial and angular coordinate about an arbitrary origin. Upon substitution of Eq. 3 into Eq. 1, we find the bending energy  $\tilde{E} \sim b \sum_{n=2}^{\infty} (a_n^2 + b_n^2)$ . To determine  $a_n$ ,  $b_n$ , we solve  $\nabla_{\perp}^2 h(r, \theta) = H(r, \theta)$  and impose boundary conditions (see Appendix A) on  $h(r, \theta)$  at  $\mathbf{C}$ . In the limit of small noncircularity or low protein concentrations, the largest nondivergent terms are associated with  $n = 2$ . Wiggly inclusion cross-sections or highly oscillating boundary conditions only weakly affect membrane bending-mediated protein–protein interactions via  $n > 2$  terms. We derive the full multibody, interaction energy in Appendix A. The two-body interaction energy measured in units of  $k_B T$  is

$$E(R, \theta_1, \theta_2; \Delta, K_b, \Omega) = \left| \frac{e^{-2i\Omega}}{R^2} + K_b - \frac{\Delta}{2} e^{-2i\theta_1} \right|^2 + \left| \frac{e^{-2i\Omega}}{R^2} + K_b - \frac{\Delta}{2} e^{-2i\theta_2} \right|^2. \quad (4)$$

The dimensionless separation distance  $R$ , protein ellipticity  $\Delta$ , and background curvature  $K_b$  are given by

$$R \equiv \frac{r}{R_0}, \quad R_0 \equiv a \sqrt{\gamma B}^{1/4}, \quad \Delta \equiv \bar{\varepsilon} \sqrt{B},$$

$$K_b \equiv a \sqrt{B} \left( \frac{\partial^2 h_b(x_1, x_2)}{\partial x_1^2} \right), \quad (5)$$

where  $B \equiv \pi b/k_B T$  is the dimensionless bending stiffness, and  $\bar{\varepsilon} \sim O(\varepsilon)$  quantifies the noncircular nature (shape, contact height, or contact angle ellipticity), of each inclusion (see Appendix A). The angle  $\Omega$  is measured between the line joining the protein centers and the principle axis of curvature defined by the background Gaussian curvature (see Fig. 3). The angles  $\theta_1$ ,  $\theta_2$  are measured between the principle axes of proteins 1 and 2 and the same principle axis. The quantity  $K_b$  measures the local, externally induced (via other distant proteins or external bending forces) background curvature in this principle axis direction. We show in Appendix A that the dominant effect of distant proteins is to induce mean curvature deformations that decay as  $1/r^2$ , but constant negative Gaussian curvatures. The local curvature  $K_b$  arises only from deformations that are of zero mean curvature. Our analyses will be applied to the pair interaction energy given by Eq. 4 with the convention  $\Delta, K_b \geq 0$ .

## ROTATIONALLY AVERAGED INTERACTIONS

Proteins that are not attached to the cytoskeleton are free to rotate and diffuse within the membrane. The interaction potential between two membrane-deforming inclusions is a complicated function of their relative angles and separation distance (cf. Eq. 4). Although the energy is a function of the specific separations and angles between two membrane-associated proteins, their rotational time scales are less than, or comparable to their translational diffusion time scales so that one can average over the rotational degrees of freedom, as the following argument demonstrates.

A small solvent molecule in solution has a rotational correlation time of the order  $\tau_{\text{rot}} \lesssim 1$  ns, while its translational diffusion constant is  $D_{\text{trans}} \sim 10^{-6}$  cm<sup>2</sup>/s. Therefore, in the time it takes for a small solvent molecule to lose rotational correlation,  $\tau_{\text{rot}}$ , it would have translated

$$\delta r \sim \sqrt{\tau_{\text{rot}} D_{\text{trans}}} \lesssim 0.1 \text{ nm}. \quad (6)$$

Similarly, for membrane constituents, such as bilayer lipid molecules and small membrane proteins,  $\tau_{\text{rot}} \sim 1$ –5 ns, and  $D_{\text{trans}} \sim 10^{-8}$ – $10^{-7}$  cm<sup>2</sup>/s, where  $\tau_{\text{rot}}$  corresponds to rotation about the molecular axis parallel to the normal vector of the membrane (Marsh, 1990). As with small molecules in bulk solution, membrane-bound lipid molecules also move  $\delta R \sim 0.1$  nm during a rotational correlation time. Protein rotational correlation times increase as  $a^3$ , whereas  $D_{\text{trans}}$  decreases with  $a$ . Membrane proteins that are not too large

may only diffuse  $\delta r \sim 1$  nm during the time over which it has lost rotational correlation. Therefore, in the time it takes for a typical inclusion to rotate about its axis, it has diffused no more than its own diameter. This estimate is consistent with fluorescence measurements that find  $\tau_{\text{rot}} \sim 0.1\text{--}1$  ms (Yamada et al., 1999). However, rotational time scales for larger proteins may not be much faster than translational motions; therefore, our approach of averaging rotational degrees of freedom is still valid only if we interpret the resulting effective pair interaction as a statistical weight, determining expected protein separations for *any* given relative orientation  $\theta_1 - \theta_2$ .

Rotational effects are implemented by statistically averaging over the principle axis angles of the two inclusions while keeping the distance  $R$  and angle  $\Omega$  between them fixed. We weight the exact two particle energy over its own Boltzmann weight according to

$$E_{\text{eff}}(R; \Delta, K_b, \Omega) = Z^{-1} \int_0^{2\pi} \int_0^{2\pi} E(R; \Delta, K_b, \theta_1, \theta_2) e^{-E(R, \theta_1, \theta_2; \Delta, K_b, \Omega)} d\theta_1 d\theta_2, \quad (7)$$

where the rotational partition function

$$Z \equiv \int_0^{2\pi} \int_0^{2\pi} e^{-E(R, \theta_1, \theta_2; \Delta, K_b, \Omega)} d\theta_1 d\theta_2. \quad (8)$$

Upon substitution of Eq. 4 into Eqs. 7 and 8, and performing the integration (see Appendix B),

$$E_{\text{eff}}(R; K_b, \Omega) = \frac{2\xi^2}{\Delta^2} + \frac{\Delta^2}{2} - 2\xi \frac{I_1(\xi)}{I_0(\xi)}, \quad (9)$$

where

$$\xi = \Delta \sqrt{\frac{1}{R^4} + \frac{2K_b}{R^2} \cos 2\Omega + K_b^2}. \quad (10)$$

The effective interaction of two inclusions is defined by the difference between the membrane-bending energies of two inclusions separated at distance  $R$  and at infinite separation,

$$U_{\text{eff}}(R; \Delta, K_b, \Omega) = E_{\text{eff}}(R; \Delta, K_b, \Omega) - E_{\text{eff}}(\infty) = \frac{2\xi^2}{\Delta^2} - \frac{2\xi I_1(\xi)}{I_0(\xi)} - \left[ 2K_b^2 - 2\Delta K_b \frac{I_1(\Delta K_b)}{I_0(\Delta K_b)} \right]. \quad (11)$$

For fixed ellipticity  $\Delta$ , the set of parameters  $K_b$ ,  $\Omega$ , and  $R$  that gives rise to a minimum at  $R^* < \infty$ , if it exists, is

implicitly determined by

$$\left( \frac{\partial U_{\text{eff}}}{\partial R} \right)_{R^*} = 0, \quad (12)$$

for sufficiently small  $R$ ,  $U_{\text{eff}} \approx 2/R^4$ , as in the circular protein case.

### Zero background curvature

First, consider the case of two isolated proteins embedded in a flat membrane. In the absence of external mechanical forces that impose background membrane deformations, and with other inclusions sufficiently far away,  $H_b = K_b = 0$ , and  $\xi = |\Delta|/R^2$ . The effective potential (Eq. 11) becomes

$$U_{\text{eff}}(R; \Delta, K_b = 0) = \frac{2}{R^4} - \left( \frac{2\Delta}{R^2} \right) \frac{I_1(\Delta/R^2)}{I_0(\Delta/R^2)}. \quad (13)$$

Without background curvature ( $K_b = 0$ ), there are no defining principle axes, and  $U_{\text{eff}}$  is independent angle. From Eq. 13, we see that an effective attractive interaction can arise for  $\Delta/R^2 \gg 1$ , when  $I_1(\Delta/R^2)/I_0(\Delta/R^2) \sim 1$ , and  $U_{\text{eff}}(R; \Delta, K_b = 0) \sim 1/R^4 - \Delta/R^2$ . Although the interaction (Eq. 4) yields both repulsive and attractive forces, the Boltzmann thermal average in Eq. 7 favors the lower energy configurations of  $\theta_1, \theta_2$ . Hence the pair of inclusions spends more time in attractive configurations, resulting in a residual attraction in  $U_{\text{eff}}(R)$ . In the  $K_b = 0$  limit, the large  $R$  behavior of Eq. 13 is

$$U_{\text{eff}}(R) = \frac{2 - \Delta^2}{R^4} + O(R^{-6}). \quad (14)$$

Because the potential becomes repulsive at short distances, an effective ellipticity  $\Delta > \Delta^* \equiv \sqrt{2}$  is necessary for the existence of a minimum in  $U_{\text{eff}}(R)$ .

Figure 2A shows the  $\theta$ -independent effective interaction potential as a function of  $R$  for various effective ellipticities  $\Delta$ . As  $\Delta$  is increased from  $\Delta^* = \sqrt{2}$ , the minimum radius  $R^*$  determined by Eq. 12, decreases rapidly from  $R^* \sim \infty$ . The  $\Delta > \Delta^*$  dependence of  $R^*$  is plotted in Figure 2B. Also shown are the corresponding magnitudes of the global minima of  $U_{\text{eff}}(R; \Delta, K_b = 0)$  as a function of  $\Delta$ .

We now estimate the numerical values of the parameters by considering specific, physiological membrane protein systems. Figure 3, A and B shows two views of the photo-reaction center membrane protein from *Rhodospseudomonas viridis* (Deisenhofer et al., 1999). The wedge angle, and hence the contact slope,  $\gamma = \tan(0.38) \approx 0.4$  is estimated by considering the coordinates of the hydrophobic, transmembrane fragments (Fig. 3C). Adsorbed proteins, or tilted peptides can even induce larger slopes  $\gamma \gtrsim 2$  (corresponding to  $\gtrsim 60^\circ$ ) (Brasseur, 2000). In what follows, we will use  $\gamma \approx 0.4$  as a value representative of certain highly asymmetric membrane proteins. The ellipticity  $\varepsilon/a \sim 0.5$  of the

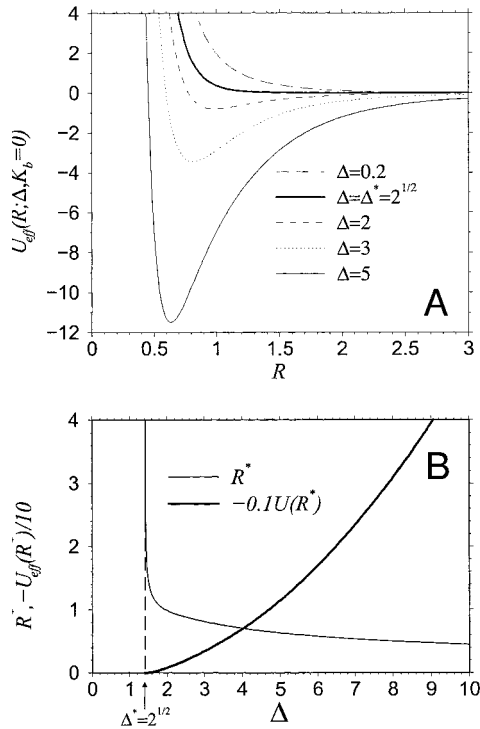


FIGURE 2 (A) Rotationally averaged effective potential (Eq. 13) as a function of protein separation in a flat membrane ( $H_b = K_b = 0$ ). (B) The minimum effective energy and its associated radius  $R^*$ . The minimum of the potential is plotted as  $1/10|U_{\text{eff}}(R^*)|$ . Note that  $R^*$  quickly decreases when  $\Delta$  increases above  $\Delta^* = \sqrt{2}$ . For large  $\Delta \gg 1$ ,  $R^* \sim \sqrt{2/\Delta}$  and  $|U_{\text{eff}}(R^*)| \sim \Delta^2/2$ .

photoreaction center is also estimated by comparing Fig. 2, A and B. (A more precise interpretation of Fig. 3, A and B, and Eq. 24 is  $\gamma \approx 0.2$ ,  $\delta\gamma \approx 0.4$ , and  $\varepsilon/a \approx 0.5$ ; however Fig. 3 serves only to provide approximate values for  $\Delta$ .) Numerous mechanical measurements have been performed to obtain the lipid bilayer bending stiffness,  $b$ . Song and Waugh (1993) mechanically measured  $b \approx 3.3 \times 10^{-19}$  J for cholesterol-loaded stearyl-oleoyl-phosphatidyl-ethanolamine (SOPC) bilayers, whereas Strey and Peterson (1995) studied thermal fluctuations of erythrocyte membranes to deduce  $b \approx 4 \times 10^{-19}$  J. Thus, for  $T = 300^\circ\text{K}$ , typical values are  $B = \pi b/k_B T \approx 300$ .

Assuming a protein-induced perturbation of the bilayer membrane arising only from the nonzero contact slope  $\gamma$ ,  $\bar{\varepsilon} \approx (\varepsilon/a)\gamma$ . Using the values associated with the photoreaction center (Fig. 3),  $\Delta \approx \bar{\varepsilon}\gamma\sqrt{B} = (0.5)(0.4)\sqrt{300} \approx 3.5$ ,  $R^* \approx 0.8$ , and  $U_{\text{eff}}(R^*) \sim -4.5(k_B T)$ . Figure 2, A and B, also show that such appreciable attractive wells typically occur at distances  $R \sim 0.7$ – $0.8$ , which corresponds to (cf. Eq. 5)  $r^*/a \approx 2$ . Therefore, elastically coupled interactions can give rise to attractive potentials with minima comparable to those deriving from short-ranged, direct forces such as van der Waals and screened electrostatic interactions. Although elastic deformations of the bilayer around a mem-

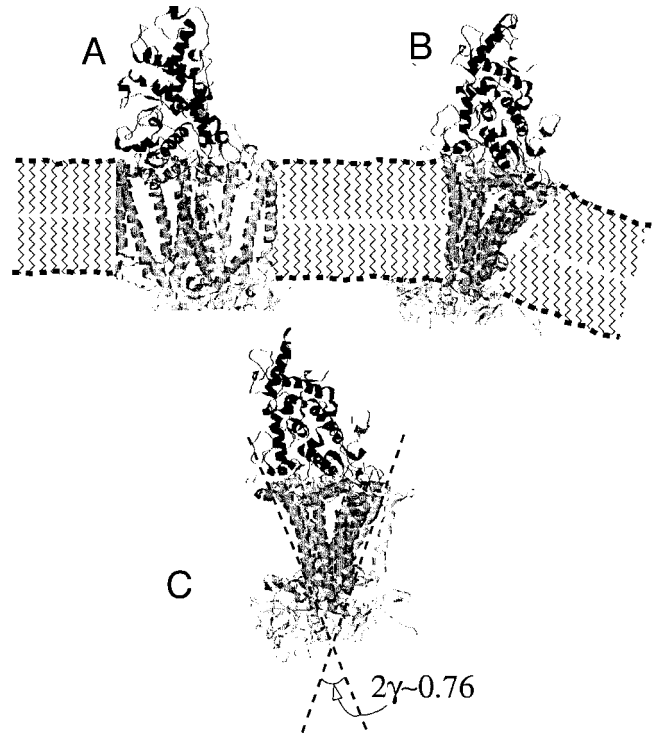


FIGURE 3 Approximate geometry of the photoreaction center of *Rhodospseudomonas viridis* (from x-ray crystal structure, (Deisenhofer et al., 1999)). The molecular coordinates of the transmembrane motifs indicate contact angles as large as 0.38, resulting in  $\gamma = \tan(0.38) \approx 0.4$ .

brane protein are long-ranged, extending as  $\ln(r)$ , the protein–protein interactions become short-ranged when rotational degrees of freedom are averaged out. This short-ranged elastic interaction can complement, or compete with, other direct molecular interactions. We conclude that thermally averaged noncircular membrane deformations can modify direct molecular interactions by at least a few  $k_B T$  at distances of  $\sim 1$ – $2$  protein radii.

### Effect of local Gaussian curvature, $H_b = 0$ , $K_b \neq 0$

Background curvature can arise due to a nonuniform distribution of distant membrane proteins or an externally imposed deformation. For example, in the experiments of Cho et al. (1999) and Discher and Mohandas (1996), a lipid neck is drawn into a pipette, creating a region near the base of the neck with a large negative Gaussian curvature. Similarly, membrane fusion and fission processes in endo/exocytosis involves intermediate shapes with constricted necks containing Gaussian curvature. These regions may be “externally” imposed by proteins involved in vesiculation (e.g., dynamin or motor proteins). The Gaussian curvature in this case may also result from lipid structural or composition changes (Schmidt et al., 1999). Therefore, curvature can couple to membrane protein or lipid shapes. Localization of

lipids with specific shapes to vesicle neck regions have been implicated in the membrane budding (Schmidt et al., 1999).

The Gaussian curvature of the membrane between the two proteins establishes local axes of principle curvature such that  $a\partial_{x_1}^2 h(x_1, x_2) = -a\partial_{x_2}^2 h(x_1, x_2) \equiv \eta_b \propto K_b > 0$ . Because we assume  $H_b = 0$ , the background deformation between the two proteins will resemble a saddle with principle curvatures of equal magnitudes (cf. Fig. 4). The rotationally averaged effective interaction,  $U_{\text{eff}}(R; \Delta, K_b, \Omega)$  will generate attractions at specific orientation angles  $\Omega$  even if  $\Delta < \Delta^*$ . This can be most easily seen by expanding Eq. 11 in powers of  $1/R$  for large  $R$ :

$$U_{\text{eff}}(R \rightarrow \infty; \Delta, K_b, \Omega) \approx \frac{A_2}{R^2} \cos 2\Omega + \frac{A_4}{R^4} + O(R^{-6}). \quad (15)$$

Explicit forms for  $A_2, A_4$  are given in Appendix A. The appearance of  $A_2 \neq 0$  when  $K_b > 0$  immediately generates a minimum. Even when ellipticity vanishes ( $\Delta = 0$ ),  $A_2 \propto K_b \cos 2\Omega < 0$  for appropriate  $\Omega$ .

The physical origin of attractions in the presence of background curvature can be readily seen by considering Fig. 4. Circular proteins situated at low regions of the saddle ( $\Omega \sim \pi/2$ ) develop attractive interactions, whereas those with  $\Omega \sim 0$  always repel. Recall from previous studies that two circular proteins repel with a  $R^{-4}$  potential (Goulian, 1993; Kim et al., 1998; Park and Lubensky, 1996; Dommersnes, 1998). This is a direct consequence of placing a second protein in the Gaussian curvature created by the first one. When the background curvature of the membrane in the region between two proteins augments the individual Gaussian curvatures around the first protein (near  $\Omega = 0$ ), the  $R^{-4}$  repulsion is also enhanced. Conversely, if the

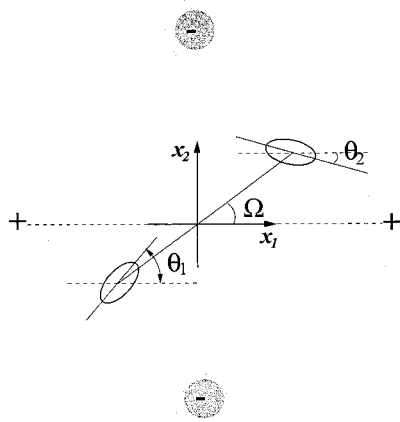


FIGURE 4 Two inclusions embedded in a local saddle deformation. The  $+/-$  correspond to raised/depressed regions of the membrane. The principle axis is aligned with the path joining the two raised regions (east-west). The principle axes of the inclusions ( $\theta_1, \theta_2$ ) and the centerline joining their centers ( $\Omega$ ) are measured with respect to this principle axis.

background curvature mitigates the saddle induced by an individual inclusion (near  $\Omega = \pi/2$ ), the other inclusion sees not only a diminished repulsion, but a mutual attraction at large enough distances. This is because the individual Gaussian curvature around a protein (arising from  $h(r) \approx -\gamma \ln(r/a)$ ) decays as  $1/r^4$  and eventually becomes smaller than the imposed constant background Gaussian curvature associated with  $K_b$ . Attractive effects of the background curvature eventually manifest themselves when  $\Omega \sim \pi/2$ .

Figure 5 A shows the effects of a small amount of local background curvature on the effective interaction potential. For small ellipticity,  $\Delta \ll \Delta^*$ , minima can still appear for large enough angles  $\Omega$  (approximately for  $\Omega > \pi/4$ ). Even for a modest value of  $\Delta = 0.3$ , corresponding to say,  $\varepsilon/a \sim 0.2$ ,  $\gamma \sim 5^\circ = 0.087$ , small attractive interactions can exist provided  $\Omega \approx \pi/2$ . For similar background curvatures but much larger ellipticities, the potential develops a repulsive barrier before becoming attractive for certain  $\Omega$ . This sig-

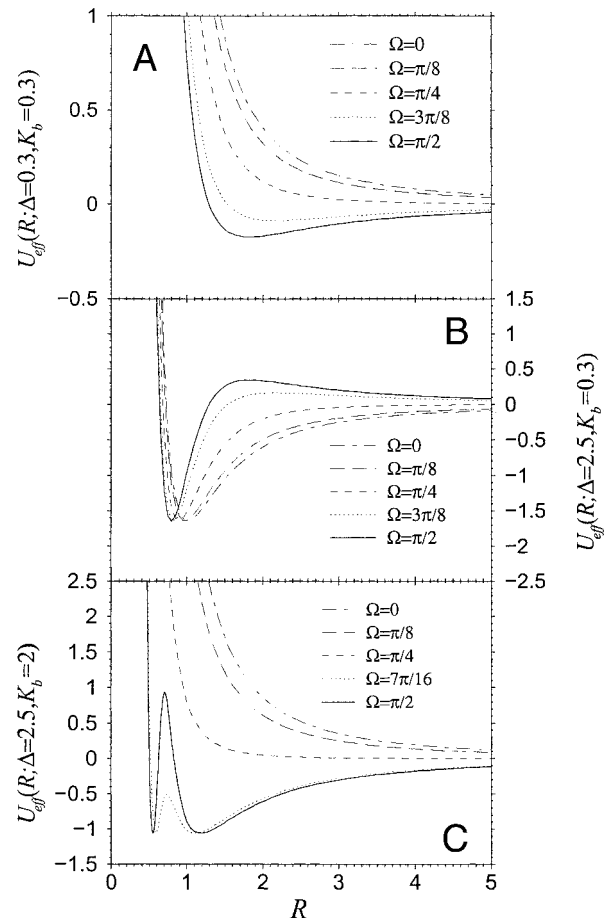


FIGURE 5 Effective potentials between two inclusions embedded in an  $H_b = 0$  and constant  $K_b$  membrane. (A)  $\Delta = 0.3$ ;  $K_b = 0.3$  for various  $\Omega$ . (B)  $\Delta = 2.5$ ;  $K_b = 0.3$ . (C)  $\Delta = 2.5$ ;  $K_b = 2$ . This latter case, although extreme under physiological conditions, yields two energy minima which are physical manifestations of the qualitatively different minima depicted in (A) and (B).

nals that  $A_4 < 0$  for large enough  $\Delta$  and is depicted in Fig. 5 B for  $\Delta = 2.5$ . In the limit of small  $K_b$ ,  $A_4 < 0$  when

$$\Delta > \Delta^* + \frac{K_b^2}{8} \left( 3 + \frac{\sqrt{2}}{2} (3 + \sin^2 2\Omega) \right) + O(K_b^4). \quad (16)$$

Figure 5 C shows that there is yet an additional, qualitatively different feature of  $U_{\text{eff}}(R; \Delta, K_b, \Omega)$  when both  $\Delta$  and  $K_b$  are large. Although typical values of  $K_b$  (see Eq. 5) in biological settings is  $K_b \ll 1$ , we find that large values of  $K_b$  and  $\Delta$  give rise to double minima in the interaction potential, especially near  $\Omega \approx \pi/2$ . Figure 5 C shows double minima for  $\Omega = 7\pi/16, \pi/2$ . Additional higher-order coefficients such as  $A_6/R^6$ , etc. are required to quantitatively describe multiple minima. The two minima are a consequence of the two independent physical effects that prefer energy minima; local Gaussian curvature associated with  $K_b$  and effective ellipticity  $\Delta$ . Typically, the weaker, longer-ranged minimum is predominantly the signature of a large  $K_b$ , whereas the deeper, shorter-ranged minimum (such as that shown in Figs. 2 A and 5 B) is a feature of ellipticity  $\Delta > \Delta^*$ . Saddles of order  $K_b > 1$  correspond to principle radii of curvature on the order of  $\sim 10$  times the protein size  $a$ , and are thus regions of extreme Gaussian deformations. Regions of such warp may only exist in transient, small systems such as fusion necks. Henceforth, we will restrict ourselves to  $K_b$  small enough to only induce one minimum.

Angles  $\Omega$ , which yield attractive interactions, can be estimated by considering  $A_2, A_4$ . Assuming  $A_4 > 0$ , values of  $A_2 < 0$  give attractive interactions when  $-\pi/4 < \Omega < \pi/4$ . When  $A_2 > 0$ , proteins with orientation  $\pi/4 < |\Omega| < 3\pi/4$  will experience attractive forces. However, these conditions are modified if  $A_4 < 0$ , when some angles within  $-\pi/4 < \Omega < \pi/4$  can yield attraction even if  $A_2 > 0$ . This case corresponds to Fig. 5 B, where a repulsive barrier at  $R > R^*$  arises. A minimum can still arise even at angles where  $A_2 \cos 2\Omega > 0$  due to the  $-R^{-4}$  behavior. The matching to repulsive behavior at smaller  $R$  requires consideration of  $+R^{-6}$  terms.

The top panel of Fig. 6 shows the radius corresponding to the only minimum of the effective potential  $U_{\text{eff}}$  as a function of  $K_b$ , for  $\Delta = 0.5, 2$ , and  $4$ . Both east–west and north–south configurations are shown, with intermediate angles  $\Omega$  interpolating between the curves. For small ellipticity, the local principle curvature  $K_b$  is the predominant source of attraction at larger distances, shown by the thick dashed curve. Increasing  $K_b$  destabilizes the effective energy minima near  $\Omega = 0$ . Above a certain background Gaussian curvature intensity, the effective potential minimum evaporates to  $R^* \rightarrow \infty$  for proteins situated at  $\Omega = 0$  (solid curves), and the attraction is washed out. For small  $K_b$ , the two effects, ellipticity and background Gaussian curvature, complement each other near  $\Omega = \pi/2$  in reinforcing an energy minimum. Consistent with Fig. 2 A for

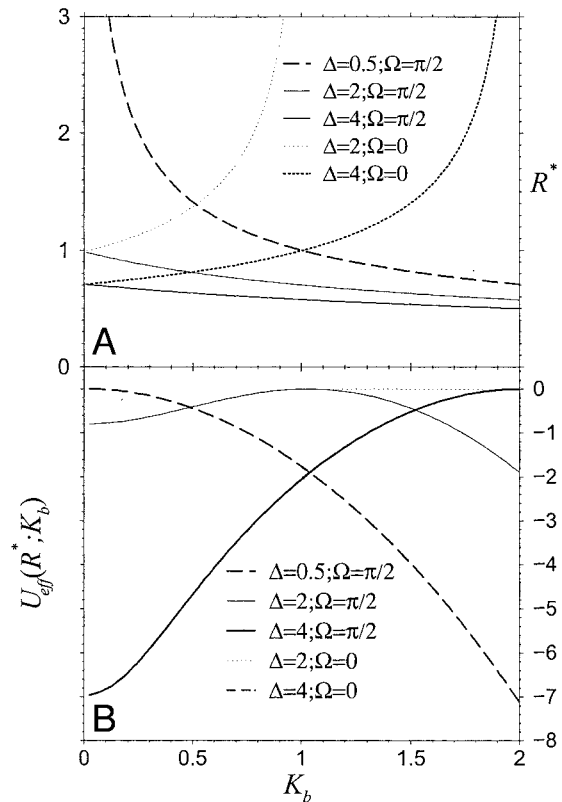


FIGURE 6 (A) The radii corresponding to interaction potential minima as a function of  $K_b$  for  $\Delta = 0.5, 2, 4$  and  $\Omega = 0, \pi/2$ . Curves that diverge signal a loss of the minimum (minimum radius  $R^* \rightarrow \infty$ ) for parameters beyond those indicated. (B) The corresponding potential energy well depths at  $R^*$ . The energies associated with  $\Delta = 2; \Omega = 0$  and  $\Delta = 2; \Omega = \pi/2$  separate at  $K_b \approx 1.1$  when the  $\Omega = 0$  energy well disappears. The minimum energies associated with large  $\Delta$  and  $\Omega = \pi/2$  is still increasing for  $K_b \geq 1.1$ .

$\Delta > \sqrt{2}$ ,  $R^*$  in Fig. 6 (thick curves) is smaller for larger  $\Delta$ . The bottom panel plots the corresponding minimum energies.

The  $\Omega$ -dependence of  $R^*$  and the minimum energy is shown in Fig. 7. As expected, for large  $\Delta \gg \sqrt{2}$ , both  $R^*$  and  $U_{\text{eff}}(R^*, \Omega)$  are fairly insensitive to  $\Omega$ . When  $\Delta$  is small, the energy minima and their associated radii  $R^*$ , caused predominantly by  $K_b$ , are very sensitive to orientation  $\Omega$ . These behaviors are consistent with the energy profiles shown in Fig. 5 B. In fact, for small enough  $\Delta$ , the minima near  $\Omega \approx 0$  are annihilated, independent of  $K_b$ . Thus, we see a qualitative difference between attractive potentials generated by intrinsic ellipticity and background Gaussian curvature.

## THE SECOND VIRIAL COEFFICIENT

We now consider the influence of the effective protein–protein attractions on a low density ensemble of inclusions. By analogy with the molecular origins of the osmotic second virial coefficients of proteins in solution (Neal et al.,

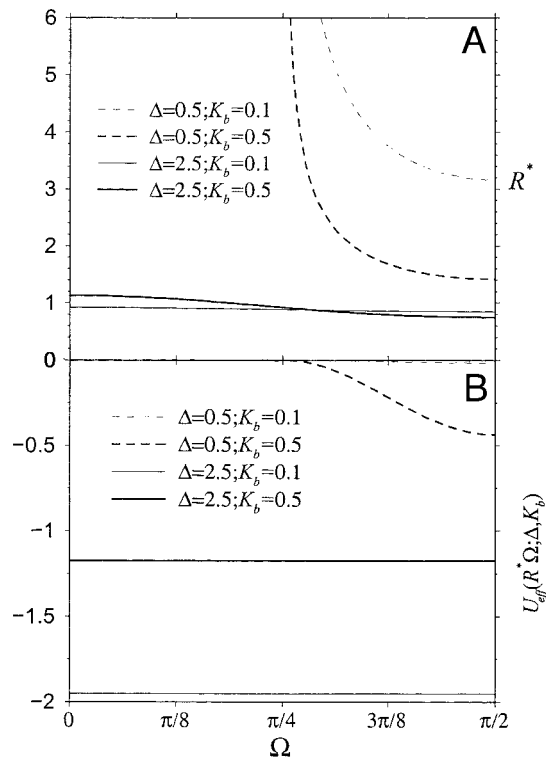


FIGURE 7 Angular dependence of (A)  $R$ , and (B)  $U_{\text{eff}}(R^*, \Omega)$  as functions of pair orientation angle  $\Omega$ . Minima arising mainly from background saddle (sensitive to  $\Omega$ ) and ellipticity (insensitive to  $\Omega$ ) are shown.

1998), we will consider the bending energy contributions to the second virial coefficient for a 2D protein equation of state. The membrane-mediated interactions are, however, much longer-ranged than those in solution (Neal et al., 1998). Consider the thermodynamic limit and times long enough such that

$$\tau \gg \frac{\ell^2}{D_{\text{trans}}} \geq \tau_{\text{rot}}, \quad (17)$$

where  $D_{\text{trans}}$  is the protein translational diffusion constant. On the time scale  $\tau$ , the inclusions are relatively free to diffuse about the bilayer. They interact among themselves via the rotationally averaged potential  $U_{\text{eff}}$  that manifests itself on time scales  $\geq \tau_{\text{rot}}$ . For very low protein densities (large protein separation  $\ell$ ), the 2D protein osmotic pressure will be nearly that of an ideal gas, analogous to a low-density gaseous-phase surfactant monolayer at the air–water interface. Finite protein size  $a$ , and longer-ranged elastically coupled interactions will give nonideal properties. The first correction to ideality in the equation of state is given by the second virial coefficient (McQuarrie, 1976),

$$\frac{\Pi}{k_B T} = \Gamma + B_2 \Gamma^2 + O(B_3 \Gamma^3), \quad (18)$$

where  $\Gamma$  is the surface concentration of protein and  $B_2$  is computed using the formula  $B_2(\Delta, K_b) \equiv -(1/2A_T)(Z_2 - Z_1^2)$  where  $A_T$  is the total area, and  $Z_1, Z_2$  are the one- and two-particle partition functions, including all internal degrees of freedom (i.e.,  $\theta_1, \theta_2$ ), respectively. The derivation of  $B_2$  is outlined in Appendix C.

The second virial,  $B_2$ , represents the small fraction of pairwise interacting proteins. Here, we do not consider how integrating out the rotational degrees of freedom affect the fixed translational degree of freedom. Instead, we are considering times long enough for equilibration of both degrees of freedom, and their combined contribution to the equation of state via  $B_2$ .

The physical origin and value of  $K_b$  used in computing particle–particle interactions and hence  $B_2$  (Eq. C1) is as follows. The local curvature felt by the interacting pair represents an interaction between this pair and some other distant proteins. However, the virial equation of state (Eq. 18) is a systematic expansion in surface density expanded about an ideal, noninteracting ensemble. Because membrane bending-mediated interactions are not pairwise additive (Kim et al., 1998), one might be tempted to assume that the presence of other proteins would modify the interaction energy  $E$  used in the expression for  $B_2$ . However, these more complicated interactions would depend upon the concentration of the other background proteins, and would generate terms of higher order in  $\Gamma$ . In other words, we start at densities so low that the protein ensemble is completely noninteracting. As the density is slightly increased, a pair of protein molecules occasionally interacts and perhaps forms dimers, with each pair ignorant of any other protein. At this still rather low density, the probability that three or more proteins approach each other is negligible. When the density is further increased, one needs to consider the higher-order virial terms. Therefore, to second order in  $\Gamma$ , the deviation of the equation of state from ideality is completely determined by the two-body interaction  $E(R, \theta_1, \theta_2; \Delta, \bar{K}_b, \Omega)$  and is independent of nonpairwise effects (McQuarrie, 1976). Note however, that the two-body interaction will depend only on  $\bar{K}_b$  associated with externally forced, zero mean curvature membrane deformations. Therefore, for the expansion Eq. 18 to be consistent, the value of  $K_b = \bar{K}_b$  to be used in Eq. C1 is that owing solely to external force-generated Gaussian curvatures, independent of the protein density.

Figure 8 A shows the numerically computed second virial coefficient as a function of inclusion ellipticity for various  $\bar{K}_b$ . As expected for small  $\bar{K}_b$ , the virial coefficient becomes increasingly negative as the ellipticity increases. The value for circular inclusions  $B_2(\Delta = 0, \bar{K}_b = 0) = \pi^{3/2}/\sqrt{2}$  corresponds to purely repulsive disks with mutual interaction  $U(R) = 2/R^4$ . At ellipticity  $\Delta \approx 2.35$ ,  $B_2(2.35, \bar{K}_b = 0) \approx 0$  corresponding to a protein solution that is ideal to second order in surface density. Although, when  $\Delta \approx 2.35 > \Delta^* = \sqrt{2}$ ,  $U_{\text{eff}}$  has an attractive minimum, its

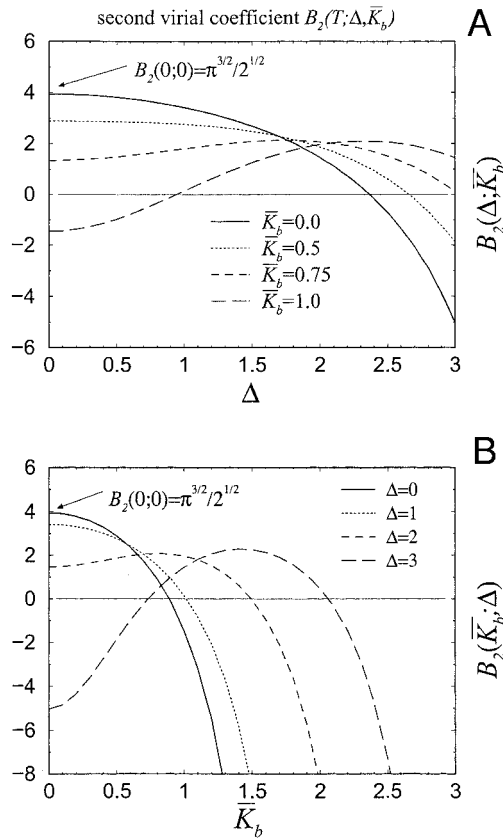


FIGURE 8 (A) Second virial coefficient  $B_2(\Delta, \bar{K}_b = 0, 0.5, 0.75, 1)$ . A negative virial coefficient is indicative of an overall attractive interaction such that the osmotic pressure is reduced from that expected in ideal solutions. The value  $B_2(0, 0) = \pi^{3/2}/\sqrt{2} > 0$  corresponds to the virial coefficient of circular, repulsive ( $U = 2/R^4$ ) inclusions. (B)  $B_2$  as a function of background saddle for various ellipticity parameters  $\Delta$ .

effects are statistically washed out by the repulsive  $R^{-4}$  part of the interaction such that the overall, effective contribution to  $B_2$  vanishes. For  $\Delta > 2.35$ , the effective attraction between membrane proteins begins to manifest itself in terms of the 2D protein osmotic pressure. The second virial is modified by externally imposed Gaussian curvature. Recall that, when  $\bar{K}_b \neq 0$ , certain angles  $\Omega$  lead to attractive interactions, even for small  $\Delta < \Delta^*$ . Because we are now thermodynamically averaging over protein positions and  $\Omega$  in addition to  $\theta_1, \theta_2$ , the inclusions will spend more time at attractive, lower energy angles  $\Omega$ , hence lowering  $B_2$ . Consistent with Fig. 5, larger values of  $\bar{K}_b$  for  $\Delta > \Delta^*$  lead to stronger repulsions at small  $\Omega$ , which average into  $B_2$ , making it less negative.

The dependence of  $B_2$  on  $\bar{K}_b$  is indicated in Fig. 8 B. For  $\Delta > 0$ ,  $B_2$ , found from numerical integration of the full expression Eq. C1, are also shown in Fig. 8 B. For  $\bar{K}_b = 0$ , increasing ellipticity decreases inclusion repulsions and  $B_2$ . As in Fig. 8 A, large  $\bar{K}_b$  and  $\Delta$  tend to increase  $B_2$ .

Equation 4 was used in Eq. C1 to compute the curves shown in Fig. 8; thus, the protein-protein interaction was

assumed to consist of contributions only from membrane bending. The hard core, excluded area of each protein,  $\sim \pi a^2$ , can be included by modifying  $U_{\text{eff}}(R)$  by setting  $U_{\text{eff}}(R \leq a/R_0) = \infty$ . Although we expect this additional repulsive term to further reduce the effective sampling area of the inclusions and increase the second virial coefficient, we find that, for all reasonable values of  $R_0$ ,  $B_2$  does not change noticeably from those shown in Fig. 8. The hard core part of the potential, due to e.g., close-ranged van der Waals repulsion, is not statistically sampled by the inclusions because the membrane bending-induced interactions ( $\sim 1/R^4$ ) already keeps them far apart.

Because nonpairwise interactions manifest themselves only at third and higher order in  $\Gamma$ , we can estimate their importance by comparing  $B_2\Gamma^2$  with  $B_3\Gamma^3$ . For nonpairwise interactions to be thermodynamically relevant, it is necessary but not sufficient that the surface density

$$\Gamma \gtrsim \left| \frac{B_2}{B_3} \right|. \quad (19)$$

Although multibody interactions may be important microscopically, their effects on the low-density equation of state, cannot be resolved. Even if the density is high enough for  $B_3\Gamma^3$  to be measurable, the value of  $B_3$  is found via a four-dimensional integral over configurations of three membrane proteins. All orientations and distances will be averaged and all components of their interactions, repulsive, attractive, pairwise, and nonpairwise will be included. In other words, one cannot uniquely determine the potential  $U$  from a measurement of  $B_n$ .

## DISCUSSION AND CONCLUSIONS

Proteins slightly beyond the range of screened electrostatic or van der Waals molecular forces can exert forces on one another by virtue of the deformation they impose on the lipid bilayer. These interactions can be attractive if the proteins have a noncircular cross-sectional shape or if the local membrane deformation is saddle shaped (negative Gaussian curvature). For bending rigidities  $b \approx 100k_B T$ , and protein shape ellipticities  $\varepsilon/a \sim 0.3-0.5$ , we find attractive interactions of a few  $k_B T$  acting at a range of  $\sim 2-3$  protein radii, augmenting shorter-ranged forces such as direct van der Waal's or screened electrostatic interactions. On a flat membrane ( $H_b = K_b = 0$ ), an effective ellipticity  $\bar{\varepsilon} > (2k_B T/\pi b)^{1/2}$  is necessary for a potential minimum to emerge between a pair of proteins. We also considered an ensemble of surface proteins elastically coupled by membrane deformation and computed the deviation of its equation of state from that of an ideal solute. Although membrane-mediated protein-protein interactions are nonpairwise additive (Kim et al., 1998), only the two-particle interaction is relevant for sparsely distributed proteins. On a flat membrane, the second virial coefficient

$B_2 < 0$  when  $\bar{\varepsilon} \geq 1.32\sqrt{k_B T/b}$  ( $\Delta \approx 2.35$ ). At this ellipticity, the elastically induced  $1/r^4$  repulsive interactions just compensate for the rotationally averaged attractions. This dependence on  $b/k_B T$  suggests that the cell can regulate protein–protein interactions by varying the lipid composition and hence the bending rigidity of the bilayer, with larger bending moduli enhancing the probability of attractive interactions.

In addition to the photoreaction center, many membrane-associated proteins are composed of certain peptides that interact strongly, and are oriented in highly tilted configurations with respect to the lipid bilayer normal. Examples include the glycoporphin A dimer, and numerous viral envelope proteins implicated in inducing membrane fusion. Specific residues of the Newcastle Disease Virus have hydrophobic characteristics that give rise to tilted insertion into lipid bilayers and have estimated tilt angles as high as  $70^\circ$  (Brasseur, 2000). Recall that the stability of highly tilted integral membranes depends only on their hydrophobic matching area, a clamped boundary condition near the protein, and membrane tension (which we do not consider).

Macromolecular dimerization is ubiquitous in cell function. We theorize that bending-mediated attractions can manifest themselves in numerous aggregation/dimerization processes. If circular proteins overcome short-ranged repulsions and dimerize due to short-ranged attractions such as van der Waals interactions, barriers to further aggregation of these elliptical dimers are reduced by dimer–dimer attractions described by Eq. 11. If the inclusions are themselves dimers or higher aggregates that persist on the time scale of rotation, bending-mediated attraction would enhance further aggregation. Moreover, G-protein-linked receptors must activate nearby membrane-associated G-proteins, which themselves may dissociate after activation (Alberts et al., 1994; Iniguez-Lluhi et al., 1993). A membrane-mediated elastic interaction, especially one with two minima (in the presence of external Gaussian curvature) may keep the necessary signaling components in close proximity. Our results in the presence of background curvature ( $K_b \neq 0$ ) also suggest that receptor activity may depend on its spatial location with respect to regions of local Gaussian curvature, such as fusion necks.

Our results suggest potential experiments in artificial membrane systems where intrinsic parameters can be controlled and surface density can be made small enough for a virial expansion to be valid. Although the 2D osmotic pressure would be difficult to measure accurately, measurements of the association time between dimerized proteins are feasible. Measurements have been made of the lifetimes of gramicidin A channels composed of dimers of barrels in opposite bilayer leaflets as a function of bilayer thickness (Kolb and Bamberg, 1977; Elliot et al., 1983). Measurements of dimer lifetimes as a function of lipid tail length  $d/2$  (the bending modulus  $b \propto d^3$ ), as well as externally imposed Gaussian deformations, may reveal the dependence of the

attractive interactions outlined in this paper. Even though an imposed Gaussian curvature increases the interaction well depth at  $\Omega \approx \pi/2$ , and destroys the attractions for proteins near  $\Omega \approx 0$ , the overall statistical effect, is to enhance binding, as is evident from Fig. 8. Therefore, we expect that dimer lifetimes can be enhanced for proteins residing in regions of large magnitudes of Gaussian curvature such as the base of extruded tubules. This may be instrumental in recruiting fusagens to the correct location for membrane budding. Finally, we remark that numerous experiments use immuno-gold particles to track membrane proteins such as coagulation enzymes (McGee and Teuschler, 1999) and synaptic junction  $\gamma$ -amino butyric acid (GABA) receptors (Nusser et al., 1998). The dimerization/aggregation frequently observed may be a consequence of bilayer deformations induced by the membrane-bound gold colloids, as demonstrated in the experiments of Koltover et al. (1999).

## APPENDIX A: INTERACTION ENERGY AMONG NONCIRCULAR INCLUSIONS

We consider the boundary conditions that the height,  $h(r, \theta)$ , must satisfy and the effects of noncircular proteins on the interaction energies (Kim et al., 1999). Consider proteins with chemistry that changes the cross-sectional protein shape from circularity by an amount  $\varepsilon$ . The concomitant changes in lipid contact height and angle are also assumed to be modified by  $O(\varepsilon)$ . As shown in Fig. 1, the protein perimeter, measured from the protein center is, to order  $O(\varepsilon)$ ,

$$\mathbf{C} \simeq (a + \varepsilon \cos 2(\theta - \theta_i))\mathbf{n}, \quad (\text{A1})$$

where  $\mathbf{n}$  is the unit normal vector to the curve  $\mathbf{C}$  projected onto the bilayer midplane, and  $\varepsilon \cos 2(\theta - \theta_i)$  is a small, angle-dependent perturbation measuring the deviation from circularity of protein  $i$ . Upon expanding the general boundary conditions  $h(\mathbf{C}) = \delta h(\theta)$  and  $\mathbf{n} \cdot \nabla h(\mathbf{C}) = -\gamma - \delta\gamma(\theta)$  to lowest order in  $\varepsilon$ , we arrive at effective boundary conditions,

$$\begin{aligned} h(a) &\simeq \delta h(\theta - \theta_i) + \gamma\varepsilon \cos 2(\theta - \theta_i) + O(\varepsilon^2), \\ \partial_r h(a) &\simeq -\gamma \left( 1 + \frac{\varepsilon}{a} \cos 2(\theta - \theta_i) \right) \\ &\quad - \delta\gamma(\theta - \theta_i) + O(\varepsilon^2), \end{aligned} \quad (\text{A2})$$

where we have for simplicity also assumed the variations  $\delta h(\mathbf{C})$  and  $\delta\gamma(\mathbf{C})$  to be also of order  $\varepsilon$ .

In the limit of small noncircularity or low protein concentrations, the dominant nondivergent contribution of  $H(\mathbf{r})$  to the energy  $\bar{E}$  is  $a_2^2 + b_2^2$ . The deformation  $h(r, \theta)$  that satisfies  $\nabla^2 h(r, \theta) = 2H(r, \theta)$  and Eqs. A2 can be written in the form

$$h(r, \theta) \simeq -\gamma \ln\left(\frac{r}{a}\right) + \sum_{n=2}^{\infty} (f_n(r)\cos n\theta + g_n(r)\sin n\theta), \quad (\text{A3})$$

and determine  $a_2, b_2$ . When the proteins have intrinsic noncircularity ( $\varepsilon \neq 0$ ),  $a_2^2 + b_2^2$  turns out to be the magnitude of the local Gaussian curvature (since  $H_b = 0$ ), modified by additional  $\theta_i$ -dependent terms (Kim et al., 1999). The local Gaussian curvature due to the other  $j$  far field proteins, in either case, is calculated using the leading order term  $h(\vec{r}) \approx -\gamma \ln|\vec{r} - \vec{r}_j|$ , which is simply a superposition of the longest-ranged  $\ln r$  terms about each

inclusion. The total bending energy  $\tilde{E}[H(r, \theta)]$  for an ensemble of  $N$  inclusions can be written in the complex form (Kim et al., 1999),

$$\tilde{E} = \pi b \gamma^2 \sum_j \left| \sum_{i \neq j} \frac{a^2}{(z_i - z_j)^2} - \frac{\bar{\varepsilon}}{2\gamma} e^{-2i\theta_j} \right|^2, \quad (\text{A4})$$

where  $z_i = x_i + iy_i$  is the position of the  $i$ th protein in the complex plane, and

$$\bar{\varepsilon} \equiv \left( \frac{\varepsilon}{a} \right) \left( \gamma + 2 \frac{\delta h}{a} - \delta \gamma \right) \quad (\text{A5})$$

measures the effective ellipticity of the identical proteins. Now consider two relatively isolated, identical proteins  $i, j = 1, 2$ . The effects of proteins far away are felt via a local Gaussian curvature emanating from these background proteins. Upon explicitly separating these contributions, the pair interaction energy becomes

$$\begin{aligned} \tilde{E}(r, \theta_1, \theta_2; \eta_b, \Omega) \\ = \pi b \left[ \left| \frac{a^2 \gamma e^{-2i\Omega}}{r^2} + \eta_b - \frac{\bar{\varepsilon}}{2} e^{-2i\theta_1} \right|^2 \right. \\ \left. + \left| \frac{a^2 \gamma e^{-2i\Omega}}{r^2} + \eta_b - \frac{\bar{\varepsilon}}{2} e^{-2i\theta_2} \right|^2 \right], \quad (\text{A6}) \end{aligned}$$

where

$$\eta_b \equiv a \frac{\partial^2 h_b(\mathbf{S})}{\partial x_1^2} = -a \frac{\partial^2 h_b(\mathbf{S})}{\partial x_2^2} \quad (\text{A7})$$

is the curvature in the  $\mathbf{x}_1$  principle direction due to far-field background inclusions or externally induced deformations  $h_b \approx -\gamma \ln|z - z_j|, j \geq 3$ . The mean curvature expanded about a noncircular protein (Eq. 3) results in a deformation  $h(r, \theta)$  with terms proportional to  $r^2 \cos 2\theta, r^2 \sin 2\theta$  (Kim et al., 1998). These terms carry zero mean curvature, but constant negative Gaussian curvature. From the expansion Eq. 3, the only mean curvature contributions decay as  $r^{-2}$ , which we neglect. A further contribution to the local saddle curvature,  $\eta_b^2$ , felt by the two proteins, can arise from externally applied mechanical forces that deform the bilayer in an appropriate way. The angles  $\theta_1, \theta_2$  are the angles of the principle axes of the inclusion shape (or the height or contact angle slope functions  $\delta h, \delta \gamma$ ) measured from the principle background curvature axis  $\mathbf{x}_1$ . The angle  $\Omega$  measures the angle between the principle background curvature axis and the segment joining the centers of the two inclusions. Upon rescaling according to Eq. 5, we arrive at the energy given in Eq. 4.

## APPENDIX B: ROTATIONAL AVERAGING

The integrals

$$\int_0^{2\pi} E(R, \theta_1, \theta_2; K_b, \Omega) e^{-E} d\theta_1 d\theta_2$$

and

$$Z \equiv \int_0^{2\pi} e^{-E} d\theta_1 d\theta_2 \quad (\text{B1})$$

used to compute the rotationally averaged, effective protein–protein interaction involve integration of

$$\int_0^{2\pi} (\alpha \cos 2\theta + \beta \sin 2\theta) \exp(\alpha \cos 2\theta + \beta \sin 2\theta) d\theta$$

and

$$\int_0^{2\pi} \exp(\alpha \cos 2\theta + \beta \sin 2\theta) d\theta, \quad (\text{B2})$$

respectively. The first integral in Eq. B2 can be computed in closed form by substituting the exponents with their Bessel function expansions,

$$\begin{aligned} e^{\alpha \cos 2\theta} &= I_0(\alpha) + 2 \sum_{n=1}^{\infty} I_n(\alpha) \cos 2n\theta \\ e^{\beta \sin 2\theta} &= I_0(\beta) + 2 \sum_{n=1}^{\infty} (-1)^n I_{2n}(\beta) \cos 4n\theta \\ &\quad - 2 \sum_{n=1}^{\infty} I_{2n+1}(\beta) \sin 2(2n+1)\theta, \quad (\text{B3}) \end{aligned}$$

and integrating term by term. The cross-terms of the product of the two equations in Eq. B3 involve single powers of  $\cos$  and  $\sin$  and vanish upon integration. We are left with

$$Z^{1/2} = 2\pi I_0(\alpha) I_0(\beta) + 4\pi \sum_{n=1}^{\infty} (-1)^n I_{2n}(\alpha) I_{2n}(\beta). \quad (\text{B4})$$

An analytic continuation of the sum formula,

$$\begin{aligned} J_0(\sqrt{\alpha^2 + \beta^2 - 2\alpha\beta \cos \varphi}) \\ = J_0(\alpha) J_0(\beta) + 2 \sum_{n=1}^{\infty} J_n(\alpha) J_n(\beta) \cos n\varphi, \quad (\text{B5}) \end{aligned}$$

at  $\varphi = \pi/2$  simplifies Eq. B4 to,

$$Z^{1/2} = 2\pi I_0(\xi), \quad \xi \equiv \sqrt{\alpha^2 + \beta^2}. \quad (\text{B6})$$

Finally, the second integral in Eq. B2 can be computed by taking derivatives of  $Z^{1/2}$ ,

$$\begin{aligned} \int_0^{2\pi} (\alpha \cos 2\theta + \beta \sin 2\theta) \exp(\alpha \cos 2\theta + \beta \sin 2\theta) d\theta \\ = \left( \alpha \frac{\partial}{\partial \alpha} + \beta \frac{\partial}{\partial \beta} \right) Z^{1/2}. \quad (\text{B7}) \end{aligned}$$

Using these results, we arrive at the rotationally averaged energy  $E_{\text{eff}}$  given by Eq. 9. For large separation distances  $R$ , the effective interaction  $U_{\text{eff}}(R) \equiv E_{\text{eff}}(R) - E_{\text{eff}}(\infty)$  defined in Eq. 11 can be expanded as in Eq. 15

where the coefficients are given by

$$A_2 \equiv 4K_b - 2\Delta^2 K_b \frac{\partial}{\partial \xi} \left( \frac{I_1(\xi)}{I_0(\xi)} \right)_{\Delta K_b} - 2\Delta \frac{I_1(\Delta K_b)}{I_0(\Delta K_b)} \quad (\text{B8})$$

and

$$A_4 \equiv 2 - \Delta^2 \frac{\partial}{\partial \xi} \left( \frac{I_1(\xi)}{I_0(\xi)} \right)_{\Delta K_b} - \frac{\Delta}{K_b} \frac{I_1(\Delta K_b)}{I_0(\Delta K_b)} \sin^2 2\Omega - \Delta^2 \left[ K_b \frac{\partial^2}{\partial \xi^2} + \frac{\partial}{\partial \xi} \right] \left( \frac{I_1(\xi)}{I_0(\xi)} \right)_{\Delta K_b} \cos^2 2\Omega. \quad (\text{B9})$$

### APPENDIX C: CALCULATION OF $B_2$

Because we wish to determine the second virial coefficient and how it is manifested in the lateral pressure of a low density collection of proteins, we choose the zero of energy such that the  $\theta_1$ ,  $\theta_2$ -averaged, infinite separation two-particle energy vanishes. The second virial coefficient can be found from

$$\begin{aligned} B_2(T; \Delta, K_b) &\equiv -\frac{1}{2A_T} (Z_2 - Z_1^2) \\ &\equiv -\frac{1}{2A_T} \int d^2\vec{r}_1 d^2\vec{r}_2 d\theta_1 d\theta_2 \exp(-[E(\vec{r}_1, \vec{r}_2, \theta_1, \theta_2) - \bar{E}]) \\ &\quad + \frac{1}{2A_T} \int d^2\vec{r}_1 d^2\vec{r}_2 d\theta_1 d\theta_2 \exp \\ &\quad (-[E(|\vec{r}_1 - \vec{r}_2| = \infty, \theta_1, \theta_2) - \bar{E}]), \end{aligned} \quad (\text{C1})$$

where the separation between proteins at positions  $\vec{r}_1$  and  $\vec{r}_2$  is  $R \equiv |\vec{r}_1 - \vec{r}_2|$ . Eqs. 18 and C1 are nondimensionalized such that the surface density  $\Gamma \ll 1$  is measured by the number of proteins in area  $R_0^2$  (see Eq. 5) and the protein osmotic pressure  $\Pi$  is measured in units of  $k_B T/R_0^2$ . Eq. C1 is exact and does not require the separation of rotational and translational diffusion times needed for the derivation of  $U_{\text{eff}}(R; \Delta, K_b, \Omega)$ .

The zero of energy is defined by

$$\begin{aligned} e^{\bar{E}} &\equiv \int d\theta_1 d\theta_2 \exp(-E(|\vec{r}_1 - \vec{r}_2| = \infty, \theta_1, \theta_2)) \\ &= 4\pi^2 I_0^2(\Delta K_b) \exp(-2K_b^2 - \Delta^2/2). \end{aligned} \quad (\text{C2})$$

Hence, the second virial coefficient becomes

$$\begin{aligned} B_2(T; \Delta, K_b) &= -\frac{1}{2} \int_0^\infty R dR \int_0^{2\pi} d\Omega \\ &\quad \times \left[ \frac{I_0^2(\xi)}{I_0^2(\Delta K_b)} \exp(-2R^{-4} - 4R^{-2} K_b \cos 2\Omega) - 1 \right]. \end{aligned} \quad (\text{C3})$$

In the limits of vanishing ellipticity or background Gaussian curvature, we can perform the  $\Omega$  integration,

$$\begin{aligned} B_2(T; \Delta = 0, K_b \neq 0) &= -\pi \int_0^\infty R dR [e^{-2R^4} I_0(4K_b/R^2) - 1], \\ B_2(T; \Delta \neq 0, K_b = 0) &= -\pi \int_0^\infty R dR [e^{-2R^4} I_0^2(\Delta/R^2) - 1]. \end{aligned} \quad (\text{C4})$$

Notice that the bracketed integrands in Eq. C3 and limiting forms Eqs. C4 vanish asymptotically at large separation  $R$ :

$$\begin{aligned} \lim_{R \rightarrow \infty} \left[ \frac{I_0^2(\xi)}{I_0^2(\Delta K_b)} \exp(-2R^{-4} - 4R^{-2} K_b \cos 2\Omega) - 1 \right] \\ = \left( 1 + 2\Delta \frac{I_1(\Delta K_b)}{I_0(\Delta K_b) R^2} + O(1/R^4) \right) \\ \times \left( 1 - \frac{4K_b \cos 2\Omega}{R^2} + O(1/R^4) \right) - 1 \\ = \left( 2\Delta \frac{I_1(\Delta K_b)}{I_0(\Delta K_b)} - 4K_b \cos 2\Omega \right) \frac{1}{R^2} + O(1/R^4). \end{aligned} \quad (\text{C5})$$

We thank J. B. Keller and J. C. Neu for helpful comments and many enlightening discussions. We are also grateful to an anonymous referee for correcting an error in our calculations.

T.C. acknowledges support from the National Science Foundation (NSF) through grant DMS-9804370. K.K. is supported by a grant from the Wellcome Trust, and G.O. is supported by NSF grant DMS-9220719.

### REFERENCES

- Alberts, B., D. Bray, J. Lewis, M. Raff, K. Roberts, and J. D. Watson. 1994. *Molecular Biology of the Cell*. Garland, New York.
- Brasseur, R. 2000. Tilted peptides: a motif for membrane destabilization. *Mol. Mem. Biol.* 17:31–40.
- Cho, M. R., D. W. Knowles, B. L. Smith, J. J. Moulds, P. Agre, N. Mohandas, and D. E. Golan. 1999. Membrane dynamics of the water transport protein Aquaporin-1 in intact human red cells. *Biophys. J.* 76:1136–1144.
- Dan, N., and S. A. Safran. 1995. Solubilization of proteins in membranes. *Israel J. Chem.* 35:37–40.
- Deisenhofer, J., O. Epp, K. Miki, R. Huber, and H. Michel. 1999. Crystallographic refinement at 2.3 Å resolution and refined model of the photosynthetic reaction centre from *Rhodospseudomonas viridis*. *J. Mol. Biol.* 246:429–457.
- Diamant, H., and D. Andelman. 1999. Binding of molecules to DNA and other semiflexible polymers. *cond-mat/9910162*.
- Discher, D. E., and N. Mohandas. 1996. Kinematics of red cell aspiration by fluorescence-imaged microdeformation. *Biophys. J.* 71:1680–1694.
- Dommersnes, P. G., J. B. Fournier, and P. Galatola. 1998. Long-range elastic forces between membrane inclusions in spherical vesicles. *Europhys. Lett.* 42:233–238.
- Dommersnes, P. G., and J. B. Fournier. 1999. N-body study of anisotropic membrane inclusions: membrane mediated interactions and ordered aggregation. *Eur. Phys. J.* B12:9–12.

- Elliot, J. R., D. Needham, J. P. Dilger, and D. A. Haydon. 1983. The effects of bilayer thickness and tension on gramicidin single-channel lifetime. *Biochim. Biophys. Acta.* 735:95–103.
- Golestanian, R., M. Goulian, and M. Kardar. 1996. Fluctuation-induced interactions between rods on a membrane. *Phys. Rev. E.* 54:6725–6734.
- Goulian, M., R. Bruinsma, and P. Pincus. 1993. Long-range forces in heterogeneous fluid membranes. *Europhys. Lett.* 22:145–150.
- Helfrich, W. 1973. Elastic properties of lipid bilayers: theory and possible experiments. *Z. Naturforsch. C.* 28:693–703.
- Iniguez-Lluhi, J., Kluess, C., and A. G. Gilman. 1993. The importance of G-protein  $\beta\gamma$  subunits. *Trends in Cell Biol.* 3:230–236.
- Kim, K. S., J. Neu, and G. Oster. 1998. Curvature-mediated interactions between membrane proteins. *Biophys. J.* 75:2274–2291.
- Kim, K. S., J. Neu, and G. Oster. 1999. The effect of protein shape on multibody interactions between membrane inclusions. *Phys. Rev. E.* 61:4281–4285.
- Kolb, H. A., and E. Bamberg. 1977. Influence of membrane thickness and ion concentration on the properties of the gramicidin A channel: autocorrelation, spectral power density, relaxation and single-channel studies. *Biochim. Biophys. Acta.* 464:127–141.
- Koltover, I., J. O. Radler, and C. R. Safinya. 1999. Membrane mediated attraction and ordered aggregation of colloidal particles bound to giant phospholipid vesicles. *Phys. Rev. Lett.* 82:1991–1994.
- Landau, L. D., and E. M. Lifshitz. 1985. *Theory of Elasticity.* Pergamon Press, New York.
- Lipowsky, R., H.-G. Döbreiner, C. Hiergeist, and V. Indrani. 1998. Membrane curvature induced by polymers and colloids. *Physica.* A47: 536–543.
- Luecke, H., B. Schobert, H. T. Richter, J. P. Cartailier, and J. K. Lanyi. 1999. Structure of bacteriorhodopsin at 1.55 angstrom resolution. *J. Mol. Biol.* 291:899–911.
- McGee, M. P., and H. Teuschler. 1999. Adsorption of vitamin K-dependent proteins on live cell membranes. *Thromb. Haemostasis.* 82:93–99.
- McQuarrie, D. A. 1976. *Statistical Mechanics.* Harper & Row, New York.
- Marsh, D. 1990. *CRC Handbook of Lipid Bilayers,* CRC Press, Boca Raton, FL.
- Myat, M. M., S. Anderson, L. A. H. Allen, and A. Aderem. 1997. MARCKS regulates membrane ruffling and cell spreading. *Curr. Biol.* 7:611–614.
- Neal, B. L., D. Asthagiri, and A. M. Lenhoff. 1998. Molecular origins of osmotic second virial coefficients of proteins. *Biophys. J.* 75: 2469–2477.
- Netz, R. R., and P. Pincus. 1995. Inhomogeneous fluid membranes: segregation, ordering, and effective rigidity. *Phys. Rev. E.* 52:4114–4128.
- Nielsen, C., M. Goulian, and O. S. Andersen. 1998. Energetics of inclusion-induced bilayer deformations. *Biophys. J.* 74:1966–1983.
- Nusser, Z., N. Hájos, P. Somogyi, and I. Mody. 1998. Increased number of synaptic GABA<sub>A</sub> receptors underlies potentiation at hippocampal inhibitory synapses. *Nature.* 395:172–177.
- Park, J. M., and T. C. Lubensky. 1996. Interactions between membrane inclusions on fluctuating membranes. *J. Phys. I,* 6:1217–1235.
- Schmidt, A., M. Wolde, C. Thiele, W. Fest, H. Kratzin, A. V. Podtelejnikov, W. Witke, W. B. Huttner, and H.-D. Söling. 1999. Endophilin I mediates synaptic vesicle formation by transfer of arachidonate to lysophosphatidic acid. *Nature.* 401:133–141.
- Song, J. B., and R. E. Waugh. 1993. Bending rigidity of SOPC membranes containing cholesterol. *Biophys. J.* 64:1967–1970.
- Stegmann, T., R. W. Doms, and A. Helenius. 1989. Protein-mediated membrane fusion. *Ann. Rev. Biophys. Biophys. Chem.* 18:187–211.
- Strey, H., and M. Peterson. 1995. Measurement of erythrocyte-membrane elasticity by flicker eigenmode decomposition. *Biophys. J.* 69:478–488.
- Struik, D. J. 1961. *Lectures on Classical Differential Geometry.* Dover, New York.
- Yamada, M., Y. Ohta, T. Sakaki, Y. Yabusaki, H. Ohkawa, and S. Kawato. 1999. Dynamic mobility of genetically expressed fusion protein between cytochrome P4501A1 and NADPH-cytochrome P450 reductase in yeast microsomes. *Biochemistry.* 38:9465–9470.